Since January 2020 Elsevier has created a COVID-19 resource centre with free information in English and Mandarin on the novel coronavirus COVID-19. The COVID-19 resource centre is hosted on Elsevier Connect, the company's public news and information website.

Elsevier hereby grants permission to make all its COVID-19-related research that is available on the COVID-19 resource centre - including this research content - immediately available in PubMed Central and other publicly funded repositories, such as the WHO COVID database with rights for unrestricted research re-use and analyses in any form or by any means with acknowledgement of the original source. These permissions are granted for free by Elsevier for as long as the COVID-19 resource centre remains active.

Journal of Colloid and Interface Science 421 (2014) 103–113

Contents lists available at ScienceDirect

Journal of Colloid and Interface Science

www.elsevier.com/locate/jcis

Heteroaggregation of microparticles with nanoparticles changes the chemical reversibility of the microparticles' attachment to planar surfaces

Chongyang Shen [a,*], Lei Wu [b], Shiwen Zhang [c], Huichun Ye [a], Baoguo Li [a], Yuanfang Huang [a,*]

[a] Department of Soil and Water Sciences, China Agricultural University, Beijing 100193, China
[b] Department of Agricultural and Biological Engineering, University of Florida, FL 32611, United States
[c] School of Earth and Environment, Anhui University of Science and Technology, Huainan 232001, China

ARTICLE INFO

Article history:
Received 16 October 2013
Accepted 24 January 2014
Available online 31 January 2014

Keywords:
Nanoparticle
Microparticle
Detachment
Homoaggregation
Heteroaggregation

ABSTRACT

This study theoretically investigated detachment of homoaggregates and heteroaggregates attached on the planar surfaces at primary minima during transients in solution chemistry. The homoaggregates were represented as small colloidal clusters with well-defined structures or as clusters generated by randomly packing spheres using Monte Carlo method. The heteroaggregates were modeled as microparticles coated with nanoparticles. Surface element integration technique was adopted to calculate Derjaguin–Landau–Verwey–Overbeek (DLVO) interaction energies for the homoaggregates and heteroaggregates at different ionic strengths. Results show that attached homoaggregates on the planar surface at primary minima are irreversible to reduction in solution ionic strength whether the primary spheres of the homoaggregates are nano- or micro-sized. Heteroaggregation of nanoparticles with a microparticle can cause DLVO interaction energy to decrease monotonically with separation distance at low ionic strengths (e.g., $\leqslant$0.01 M), indicating that the heteroaggregates experience repulsive forces at all separation distances. Therefore, attachment of the heteroaggregates at primary minima can be detached upon reduction in ionic strength. Additionally, we showed that the adhesive forces and torques that the aforementioned heteroaggregates experience can be significantly smaller than those experienced by the microspheres without attaching nanoparticles, thus, the heteroaggregates are readily detached via hydrodynamic drag. Results of study provide plausible explanation for the observations in the literature that attached/aggregated particles can be detached/redispersed from primary minima upon reduction in ionic strength, which challenges the common belief that attachment/aggregation of particles in primary minima is chemically irreversible.
© 2014 Elsevier Inc. All rights reserved.

1. Introduction

Aggregation of colloidal particles is widely present in many industrial processes and in the natural environment [24]. For example, engineered nanoparticles, if not protected by steric stabilizing agents, tend to aggregate into clusters up to several microns in aquatic environments ([14,70,31,41]. Colloidal aggregation occurs when colloid collision, motivated by Brownian motion and/or external forces (e.g., gravitational force, hydrodynamic shear), results in particle–particle attachment. The aggregation that occurs in a suspension composed of similar monodisperse colloidal particles is called homoaggregation [33]. Alternatively, aggregation of dissimilar particles is referred to heteroaggregation [42].

While the process of colloidal aggregation (e.g., colloid stability) has been extensively studied [22,24], fate and transport of the formed aggregates in the aquatic environments have received very limited attention to date. In contrast, the transport of single particles in porous media has received considerable attention. Particularly, a systematical theory [i.e., colloid filtration theory (CFT)] has been developed to describe single particles' attachment, which is one of the primary factors (e.g., detachment and straining) controlling particle transport in porous media [75,49,20,21,54,10,66,58]. The CFT illustrates that particle attachment involves two subsequent steps: (i) transport of particles from bulk fluid to the vicinity of collector surfaces and (ii) chemical–colloidal interactions between particles and surfaces. The transport step is controlled by three individual mechanisms: interception,

* Corresponding authors. Fax: +86 1062733596.
E-mail addresses: chongyang.shen@gmail.com (C. Shen), yfhuang@cau.edu.cn (Y. Huang).

http://dx.doi.org/10.1016/j.jcis.2014.01.033
0021-9797/© 2014 Elsevier Inc. All rights reserved.

gravitational sedimentation, and Brownian diffusion. The chemical–colloidal interactions include van der Waals attractions, electrical double layer interactions, and short-range repulsions (e.g., hydration forces and steric repulsion). These interaction forces are described by extended Derjaguin–Landau–Verwey–Overbeek (XDLVO) theory [68,44].

Since both CFT and DLVO theory are developed for describing single particles' attachment behavior, the aggregate is commonly treated as an equivalent sphere (e.g., in terms of size, hydrodynamics, or gyration) so that these theoretical models could be used for predictions. Lin and Wiesner [41], however, showed that the colloid interaction energy for the nanoparticle aggregates is on the same order of magnitude as those for the primary particles and is significantly weaker than that for an equivalent sphere defined by the gyration radius of the aggregate. Johnson et al. [37] experimentally showed that fractal aggregates composed of microspheres can settle on average 4–8.3 times faster than predictions by calculations for impermeable or permeable spheres of identical mass, cross-sectional area, or primary particle density. They attributed the differences in settling velocities to the reason that fractal aggregates have large pores, causing smaller overall drags per total cross-sectional area.

Above literature advances understanding about colloidal aggregates' attachment behavior. The detachment of colloidal aggregates, however, has not been investigated to date. Knowledge of the mechanisms controlling colloidal aggregate's detachment is of importance in diverse engineered applications and environmental concerns [6] because detachment of aggregates can cause permeability loss in aquifers, turbidity increase in groundwater withdrawal wells, facilitated transport of contaminants in subsurface environments, etc. Considerable effort has been devoted to the investigation of detachment of single particles from collector surfaces. For example, both microscopic examinations [72] and column experiments [2,56,40] show that single particles attached in the DLVO secondary energy minima can be spontaneously released back to the bulk solution when the secondary energy minima are comparable to the average Brownian kinetic energy ($1.5kT$, where k is Boltzmann constant and T is absolute temperature). However, the release is commonly minor in a system and, for considerable particle detachment, a hydrodynamic or chemical disturbance to the system (e.g., changing flow velocity and solution chemistry, advancing/receding air–water interfaces) is requisite [5–7,1,13].

This study theoretically examined detachment of colloidal aggregates attached on the planar surfaces at DLVO energy primary minima. The colloidal aggregates were represented by packing identical spheres or by coating microparticles with nanoparticles. The surface element integration (SEI) technique was employed to calculate DLVO interaction energies/forces for the aggregates at different solution ionic strengths [8,9,41]. We showed that the aggregates of identical spheres are irreversible to reduction in solution ionic strength. The attached microspheres coated by nanoparticles can be detached from planar surfaces by decreasing ionic strengths. The coated nanoparticles also significantly decrease the adhesive forces between the microparticles and the planar surface, thus, the attached heteroaggregates are much more favored to be detached by applied forces compared to single microparticles. Additionally, we theoretically explain why viruses exhibit conservative transport behavior in the environments although small particles have low energy barriers and are readily to be attached in primary minima.

2. Theory

2.1. Generation of colloidal aggregates

Fig. 1 presents examples of colloidal aggregates generated by clustering of a number of spheres. The clusters I and II result in tetrahedral and octahedral coordination configurations, respectively. A number of studies [43,76–78,16,71,55] have developed methods to prepare aforementioned small clusters using engineered particles (e.g., gold nanoparticle and silica particle). These small colloidal clusters with well-defined structures have drawn considerable attention in recent years in colloidal self-assembly. Yi et al. [76] demonstrated that these small aggregates posses lower symmetry than the spheres from which they are made and offer the possibility of forming more complex colloidal phases and structures. The cluster III was created as an aggregate of 20 spheres obtained by randomly placing them in the lattice sites of a simple cubic lattice by the Monte Carlo method [18]. Specifically, the first sphere was placed at the origin of the rectangular coordinate system. The position of the second sphere was randomly selected out of six possibilities. To place the third and any further spheres, a sphere that was already placed in the lattice was randomly chosen. Then the position of the new sphere was selected out of six possibilities in respect of the sphere chosen. Through occupancy test, the new sphere was placed if the position selected was free. Otherwise, the search for a suitable site was repeated. The cluster IV was created by placing 18 small spheres of equal sizes on a large sphere surface. The coordinates of the sphere centers for cluster III and the coordinates of the contacts between each small sphere and the large sphere for cluster IV are given in Table 1.

2.2. Calculation of DLVO interaction energies

The SEI technique was used to calculate DLVO interaction energies between aforementioned aggregates and the planar surface. The SEI technique, developed by Bhattacharjee and Elimelech [8], can give exact evaluation of DLVO interaction energy between a single particle of any shape and a flat surface [59]. Lin and Wiesner [41] showed that, based on the principle of the SEI, it is mathematically equivalent to calculate the interaction energy between an aggregate and a flat surface by simply summing the interaction energy between each primary particle and the flat surface. Details about using SEI to calculate the interaction energy between a primary sphere and a flat surface can be found in previous studies [8,59]. Briefly, the Cartesian coordinate system was employed (see Fig. 1). The coordinate system originates from the center of the primary particle, with the z axis pointing toward the planar surface. The xy plane of the coordinate system is oriented parallel to the planar surface.

The primary sphere surface was discretized into small area elements. The total interaction energy (U) was calculated as the sum of the differential interaction energy (E) between each area element dS and the planar surface:

$$\begin{aligned} U(H) &= \sum_S E(h)\mathbf{n}\cdot\mathbf{k}\,\mathrm{d}S \\ &= \sum_A \left(E\left(H+R-\sqrt{R^2-(x^2+y^2)}\right)-E\left(H+R+\sqrt{R^2-(x^2+y^2)}\right)\right)\mathrm{d}A \end{aligned} \tag{1}$$

where H is minimum separation distance between the primary particle and the planar surface, h is local separation distance between the element dS and the planar surface, $\mathbf{n}$ is unit outward normal to the primary particle surface, $\mathbf{k}$ is unit vector along the positive z-direction, S is total surface area of the primary particle, A is total projected area of the primary particle on the planar surface, R is radius of the primary particle, and dA is the projected area of dS on the planar surface.

The interaction energy between dS and the planar surface [i.e., $E(h)$] is calculated by adding van der Waals (VDW) attraction and the constant potential double layer (DL) interaction:

$$E(h) = E^{\mathrm{VDW}}(h) + E^{\mathrm{DL}}(h) \tag{2}$$

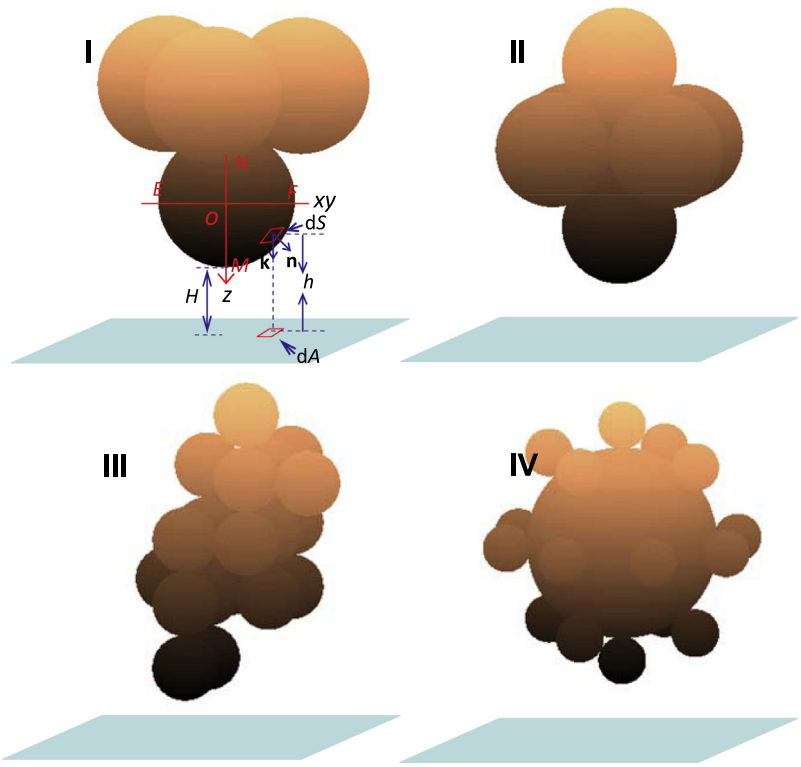

Fig. 1. Schematic of interactions of aggregates with planar surfaces. The aggregates I and II result in tetrahedral and octahedral coordination configurations, respectively. The aggregate III was created as a cluster of 20 spheres obtained by randomly placing them in the lattice sites of a simple cubic lattice by the Monte Carlo method. The aggregate IV was created by placing 18 small spheres of equal sizes on a large sphere surface. H is minimum separation distance between a primary particle and planar surface, dS is differential area element on the primary particle surface, dA is the projected area of dS on the planar surface, h is local distance of dS from the planar surface, **n** is unit outward normal to the surface and **k** is unit vector normal along the positive z-direction.

Table 1
Coordinates of the sphere centers for aggregate III and the coordinates of the contacts between each small sphere and the large sphere for aggregate IV. r, radius of the primary particles in aggregate III, R, radius of the large particle in aggregate IV. The origin of the rectangular coordinate system superposes the center of the large sphere of aggregate IV.

Aggregate III			Aggregate IV		
x	y	z	x	y	z
0	0	0	$-R$	0	0
$2r$	$2r$	$6r$	R	0	0
$-2r$	$2r$	$2r$	0	R	0
0	$2r$	$2r$	0	$-R$	0
$2r$	$2r$	$2r$	0	0	R
0	0	$2r$	0	0	$-R$
$2r$	0	$2r$	$-R/\sqrt{2}$	0	$-R/\sqrt{2}$
0	$-2r$	$2r$	$R/\sqrt{2}$	0	$-R/\sqrt{2}$
$2r$	$-2r$	$8r$	0	$-R/\sqrt{2}$	$-R/\sqrt{2}$
0	$2r$	$4r$	0	$R/\sqrt{2}$	$-R/\sqrt{2}$
$2r$	$2r$	$4r$	$-R/\sqrt{2}$	0	$R/\sqrt{2}$
0	0	$4r$	$R/\sqrt{2}$	0	$R/\sqrt{2}$
$2r$	0	$4r$	0	$-R/\sqrt{2}$	$R/\sqrt{2}$
0	$-2r$	$4r$	0	$R/\sqrt{2}$	$R/\sqrt{2}$
$2r$	$-2r$	$4r$	$R/\sqrt{2}$	$R/\sqrt{2}$	0
0	0	$6r$	$-R/\sqrt{2}$	$R/\sqrt{2}$	0
$2r$	0	$6r$	$-R/\sqrt{2}$	$-R/\sqrt{2}$	0
$4r$	$-2r$	$6r$	$R/\sqrt{2}$	$-R/\sqrt{2}$	0
0	$-2r$	0			
$2r$	$-2r$	$6r$			

The expressions used to calculate E^{VDW} and E^{DL} are following [27,30]

$$E^{\mathrm{VDW}}(h) = -\frac{A_{\mathrm{H}}}{12\pi h^2} \tag{3a}$$

$$E^{\mathrm{DL}}(h) = \frac{\varepsilon\varepsilon_0\kappa}{2}\left[(\psi_{\mathrm{p}}^2+\psi_{\mathrm{c}}^2)(1-\coth\kappa h)+\frac{2\psi_{\mathrm{p}}\psi_{\mathrm{c}}}{\sinh\kappa h}\right] \tag{3b}$$

where A_{H} is the Hamaker constant of the interacting media, ε_0 is dielectric permittivity of vacuum, ε is dielectric constant of water, κ is inverse Debye screening length, ψ_{p} and ψ_{c} are surface potentials of particle and collector, respectively.

If only van der Waals attraction and double layer interaction energies are considered, the calculated primary minimum well is infinite deep and, thus, attachment at primary minimum is irreversible. Therefore, to theoretically examine the detachment of particles from primary minima, the short-range repulsion has to be included, which was evaluated by calculating the Born potential energy in this study. The expression to calculate the Born potential energy (U^{Born}) for sphere–plane interaction can be written as follows [52]:

$$U^{\mathrm{Born}}(H) = \frac{A_{\mathrm{H}}\sigma^6}{7560}\left[\frac{8R+H}{(2R+H)^7}+\frac{6R-H}{H^7}\right] \tag{4}$$

where σ is the Born collision diameter. A typical experimentally derived value for σ is 0.5 nm [25,26]. The extended DLVO interaction energy (U_{XDLVO}) is obtained by summing U and U^{Born}.

3. Results

Unless otherwise specified, we assumed the primary particles of the aggregates and the planar surface to be negatively charged for theoretical calculations, with zeta potentials same as those of polystyrene latex particles and glass surface used in Shen et al. [60], respectively. Specifically, the zeta potentials for the latex particles were −87 mV, −81 mV, −30 mV, and −24 mV in 0.001 M, 0.01 M,

0.1 M, and 0.2 M KCl, respectively. The zeta potentials for the glass were −60 mV, −48 mV, −24 mV, and −20 mV in 0.001 M, 0.01 M, 0.1 M, and 0.2 M KCl, respectively. The value of A_H for the polystyrene-water–glass was chosen as 1×10^{-20} J [20,21,57,60].

3.1. Chemical reversibility of homoaggregates

Fig. 2 presents DLVO interaction energies between the planar surface and the tetrahedral aggregate composed of four identical spheres in Fig. 1 (aggregate I) at different solution ionic strengths. The tetrahedral aggregate is oriented with one primary sphere facing toward the planar surface and the other three primary spheres facing away from the planar surface (denoted as MIN), or oriented with three primary spheres facing toward the planar surface and the other primary sphere facing away from the planar surface (denoted as MAX). Three sizes were considered for the primary spheres of the tetrahedral cluster: 10 nm, 50 nm, and 1000 nm (in diameter). The DLVO interaction energies between the planar surface and the spheres with sizes equal to the aggregates were also shown for comparison. The interaction energy barriers are decreased for the aggregates with orientation of MIN whereas increased for the orientation of MAX compared to those of the equivalent spheres at a given ionic strength. Therefore, the DLVO interaction energy barrier is influenced by the orientation of the aggregates. Similarly, Wu et al. [74] presented that the interaction energy between a single-walled carbon nanotube and an infinite isotropic planar surface is orientation-dependent. The primary minimum depth (or detachment energy barrier from primary minimum, obtained by subtracting primary minimum from maximum energy barrier) increases with decreasing ionic strength for the aggregates with both orientations, indicating that the aggregates attached in primary minima at high ionic strengths (e.g., 0.2 M) are irreversible to reduction in solution ionic strength.

Whereas we only considered two specific orientations for the tetrahedral aggregate in Fig. 2, the attached aggregates in primary minima with other orientations are still irreversible to reduction in ionic strength (see Fig. 3). Comparison of Fig. 3 with Fig. 2 shows that the DLVO interaction energy barrier (or detachment energy barrier) reaches minimum for the orientation of MIN and maximum for the orientation of MAX. To interpret why the DLVO

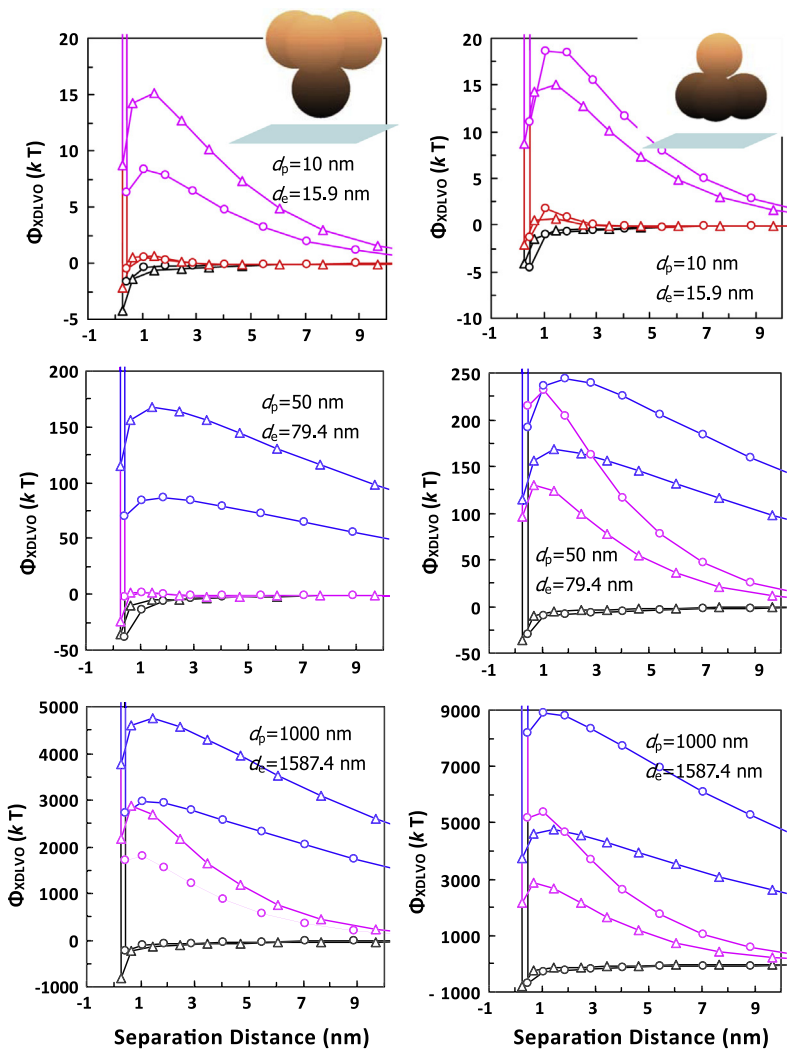

Fig. 2. DLVO interaction energies between a planar surface and the tetrahedral aggregate in Fig. 1 (solid line with circle symbol) or a sphere with size equal to the aggregate (solid line with triangle symbol) at different ionic strengths (dark, 0.2 M; red, 0.1 M; pink, 0.01 M, blue, 0.001 M). In left figures, the tetrahedral aggregate is oriented with one primary sphere facing toward the planar surface and the other three primary spheres facing away from the planar surface. In right figures, the tetrahedral aggregate is oriented with three primary spheres facing toward the planar surface and the rest primary sphere facing away from the planar surface. d_p, diameter of the primary sphere for the tetrahedral aggregate; d_e, diameter of the equivalent sphere. Some of the curves at 0.1 M or 0.001 M were not shown due to overlapping with the curves at other ionic strengths. Note the change in scale of the y axes among the various graphs. (For interpretation of the references to color in this figure legend, the reader is referred to the web version of this article.)

interaction energy barrier reaches minimum for the orientation of MIN whereas maximum for the orientation of MAX, the concept of "interaction volume" developed by Huang et al. [32] can be utilized. The interaction volume is defined as the volume between the leading surface of the particle (e.g., the aggregate in this study) and the substrate (the planar surface in this study). Obviously, the interaction volume reaches maximum for the aggregate attached on the planar surface with orientation of MIN while reaches minimum for the aggregate with orientation of MAX. In fact, the interaction volume for the orientation of MIN is larger than that for any other orientation. According to Huang et al. [32], larger interaction volume between the aggregate and the planar surface results in smaller interaction energies/forces because the mean plane of the aggregate's leading surface recedes farther from the planar surface. Hence, DLVO interaction energy/force reaches minimum for the aggregate with orientation of MIN. If the aggregate attached with the orientation of MIN cannot be detached, the aggregate attached with all other orientations cannot be detached. In the following of the paper, we only considered the interaction between the planar surface and the aggregate with orientation of MIN (i.e., the worst case).

Fig. 4 shows DLVO interaction energies for the planar surface interacting with aggregate II (i.e., the octahedral aggregate) and aggregate III (aggregate by randomly packing 20 spheres) in Fig. 1. The octahedral aggregate is oriented with its axis perpendicular to the planar surface. The orientation of the aggregate III is represented in Table 1 by the coordinates of the centers of primary spheres. The DLVO interaction energies for the equivalent spheres were also shown for comparison. Again, the increase in primary minimum depth with decreasing ionic strength illustrates that attachment of both aggregates in primary minima is irreversible to reduction in ionic strength.

Although the small clusters considered in Fig. 1 are regularly packed, the attachment of clusters is still irreversible to reduction in solution ionic strength even if they are created by randomly packing spheres (see Fig. 5). The attachment of single particles in primary minima has been shown to be irreversible to reduction in ionic strength [25,26]. The results in Figs. 2–5 consistently indicate that aggregation of identical spheres (whether they are nano- or micro-sized) does not change the chemical reversibility.

3.2. Chemical reversibility of heteroaggregates

Fig. 6 shows DLVO interaction energies between the planar surface and the aggregate IV (i.e., the heteroaggregate) in Fig. 1 at different ionic strengths. The diameter of the large sphere was assumed to be 1000 nm. Three sizes (in diameter) were considered for the small spheres: 5 nm, 10 nm, and 100 nm. The orientation of the aggregate is represented by the coordinates of the contacts between each nanoparticle and the microparticle (see Table 1). The DLVO interaction energies between the planar surface and the single microparticle were also shown for comparison. When the diameters of the nanoparticles are 5 nm and 10 nm, the primary minimum disappears from the DLVO energy curves for the aggregates at 0.01 and 0.001 M and the DLVO interaction energy decreases monotonically with increasing separation distance. This indicates that the aggregates experience repulsive forces at all separation distances, and the aggregates that are initially attached in primary minima will be detached when the solution ionic strength is decreased to ⩽0.01 M. Therefore, heteroaggregation of nanoparticles with microparticles can change the chemical reversibility of the microparticles. When the diameter of the nanoparticles is increased to 100 nm, the attachment of the aggregate becomes irreversible due to the increase in the primary minimum depth with decreasing ionic strength.

Note that in Fig. 6, the surfaces of the nanoparticles, microparticles, and the planar surface were assumed to be negatively charged. In natural environments and engineered systems, the heteroaggregates commonly consist of primary particles of different surface charges. Fig. 7 presents DLVO interaction energies

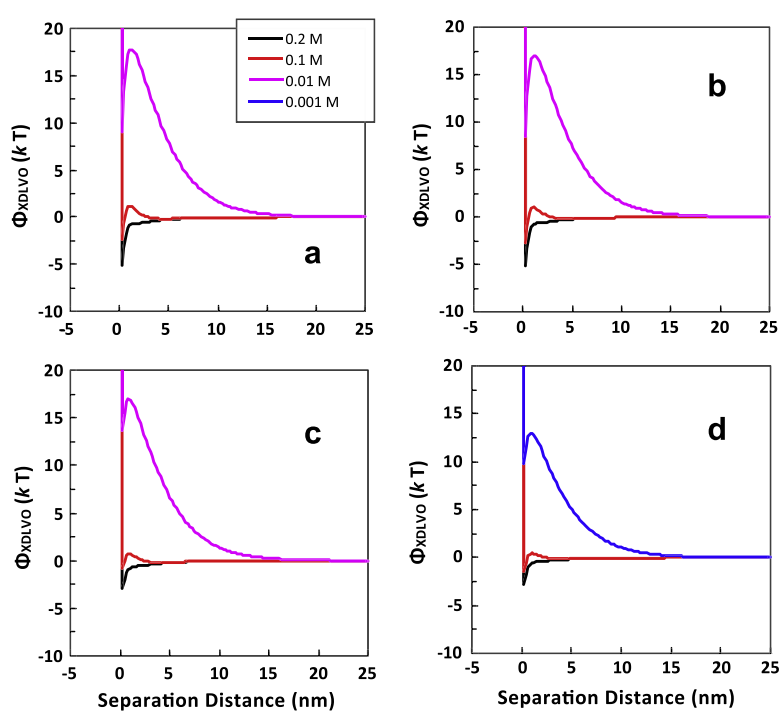

Fig. 3. DLVO interaction energies between a planar surface and the tetrahedral aggregate with different orientations at different ionic strengths. The orientation of the tetrahedral aggregate is represented in Table 2 by the coordinates of the centers of primary spheres. The diameter of the primary spheres for the tetrahedral aggregates is 10 nm. Some of the curves at 0.01 M or 0.001 M were not shown due to overlapping with the curves at other ionic strengths. Note the change in scale of the y axes among the various graphs.

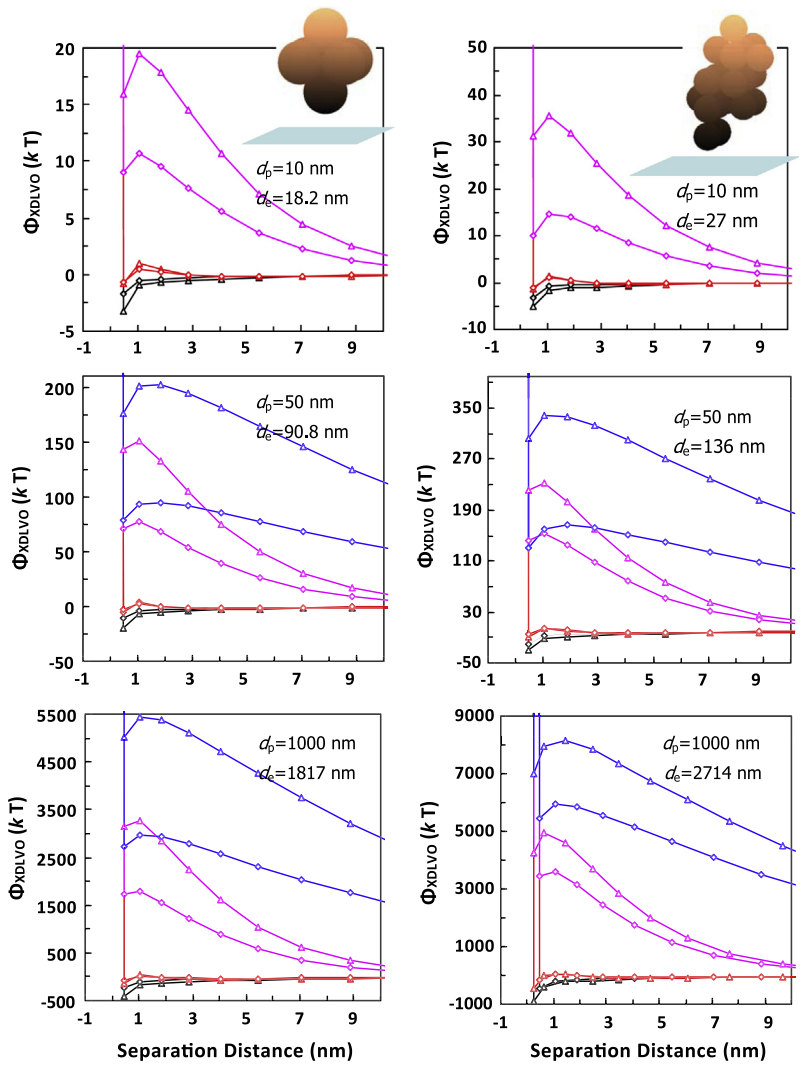

Fig. 4. DLVO interaction energies between a planar surface and the octahedral aggregate or the aggregate III in Fig. 1 (solid line with diamond symbol) at different ionic strengths (dark, 0.2 M; red, 0.1 M; pink, 0.01 M, blue, 0.001 M). In the left figures, the octahedral aggregate is oriented with its axis perpendicular to the planar surface. The orientation of the aggregate III in the right figures is represented by the coordinates of each sphere center in Table 1. The DLVO interaction energies for equivalent spheres were also shown for comparison (solid line with triangle symbol). d_p, diameter of the primary sphere for the octahedral aggregate or the aggregate III in Fig. 1; d_e, diameter of the equivalent sphere. Some of the curves at 0.001 M were not shown due to overlapping with the curves at other ionic strengths. Note the change in scale of the *y* axes among the various graphs. (For interpretation of the references to color in this figure legend, the reader is referred to the web version of this article.)

between the planar surface and the heteroaggregate in Fig. 1 with positively charged nanopartices. The nanoparticles were assumed to have zeta potentials same as those of alumina in KCl (36 mV, 25 mV, 13 mV, and 8 mV at 0.001 M, 0.01 M, 0.1 M, and 0.2 M, respectively) [23]. The zeta potentials of the glass surface and the microparticle are the same as those used in Fig. 6. Monotonic decrease in DLVO interaction energy with increasing separation distance was still observed for the aggregates with 5 nm and 10 nm nanoparticles. Thus, the attachment of the heteroaggregate in Fig. 1 in primary minima is still chemically reversible even if the nanoparticles are positively charged. When the diameter of the nanoparticles is increased to 20 nm, primary minima are present in the DLVO interaction energy curves, which increase with decreasing ionic strength, indicating irreversible attachment.

3.3. Why are the primary minima absent in the DLVO energy curves?

The classic DLVO theory only considers single particles' attachment. According to this theory, two types of interaction energy curves are present. Specifically, when the interactive surfaces are like-charged, the DLVO interaction energy curve is characterized by a deep attractive well (the primary minimum) at a small separation distance, a maximum energy barrier, and a shallow attractive well (the secondary minimum) at a larger distance (type I). Colloid attachment in the presence of repulsive interactions is termed as "unfavorable" attachment. Both energy barrier and secondary minimum disappear and only the primary minimum exists in the DLVO interaction energy curves under favorable conditions (type II). Our study shows that if the microparticle is attached by nanoparticles, the primary minima can disappear from energy curves and the interaction energy decreases monotonically with increasing separation distance at low ionic strengths (type III).

To explain why DLVO interaction energy decreases monotonically with increasing separation distance for the heteroaggregate in Fig. 1 at low ionic strengths, DLVO interaction energy profiles under different ionic strengths were calculated for the heteroaggregate in Fig. 1 (Fig. 8a), the large sphere of the heteroaggregate coated with only one small sphere at the bottom (Fig. 8b, denoted as DOUBLET), and the large sphere of the heteroaggregate only (Fig. 8c). The diameters of the large sphere and the small spheres

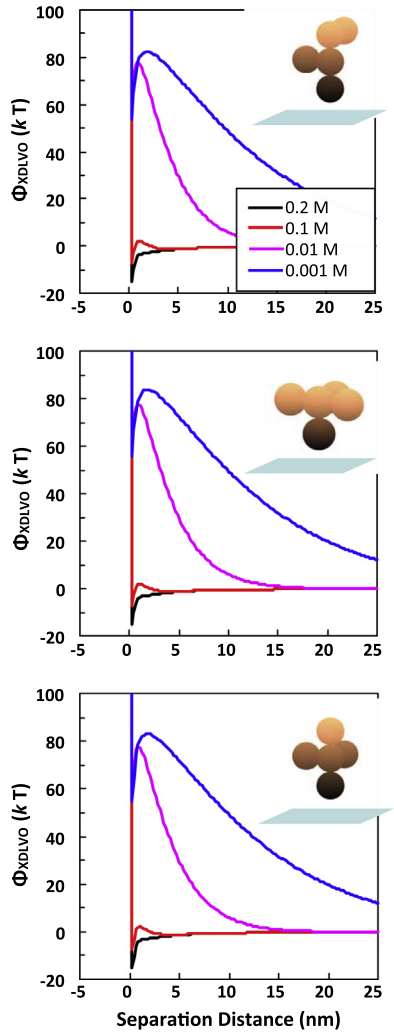

Fig. 5. DLVO interaction energies between a planar surface and aggregates at different ionic strengths. The aggregates were generated by randomly packing 5 spheres in the lattice sites of a simple cubic lattice using the Monte Carlo method. The diameter of the primary spheres for the aggregates is 50 nm. Note the change in scale of the *y* axes among the various graphs.

are 1000 nm and 10 nm, respectively. The DLVO interaction energy profiles for the heteroaggregate are very similar to those of DOUBLET, indicating that the interaction energies between the other small spheres of aggregate IV and the planar surface are negligible. This is because the DLVO interaction energies for the nanoparticle are minor compared to those for the microparticle and the interaction energy decreases rapidly with separation distance. The DLVO interaction energy profiles for the heteroaggregate and the DOUBLET are similar to the interaction energy curves for the large sphere starting from separation distance of 10 nm (i.e., σ = 10 nm) (see Fig. 8c). This indicates that the small sphere at the bottom mainly plays a role of shifting the position of the Born repulsion and, accordingly, eliminates primary minima at low ionic strengths (0.01 M and 0.001 M) or decreases primary minimum depths at high ionic strengths (0.2 M and 0.1 M). Alternatively, the absence of primary minima can be explained by the reason that the shallow primary minimum between the small sphere at the bottom and the planar surface is eliminated by the strong repulsion between the remaining part of the aggregate (mainly the microparticle) and the planar surface. The microparticle, while separated by the nanoparticle, has strong repulsion on the planar surface because the repulsive double layer interaction energy decays much slower than the van der Waals interaction energy at low ionic strengths. When the small sphere of the heteroaggregate is increased to 100 nm in diameter, the microsphere is separated far from the planar surface and the interaction energies between the microsphere and the planar surface are minor. Meanwhile, the interaction energies between the 100 nm sphere at the bottom and the planar surface become significant. Thus, the primary minima appear again in the interaction energy curves (Fig. 8c). Because the DLVO interaction energies are minor for the small particles, the aforementioned results do not change for the heteroaggregate even if the small particles are irregularly attached on the large particle's surface.

3.4. Adhesive force and torque

Table 3 presents calculated adhesive forces that the heteroaggregate in Fig. 1 and the large sphere of the heteroaggregate experience on the planar surface at different ionic strengths using the DLVO interaction energy curves in Fig. 6. The diameter of the large sphere is 1000 nm. Two diameters were considered for the small spheres of the aggregate IV: 5 nm and 10 nm. The Derjaguin and Langbein approximations were adopted in this study to calculate adhesive forces [34,64], which was estimated as Φ_{pri}/H (where Φ_{pri} is primary minimum depth). The calculations show that coating of nanoparticles on the microparticle significantly decreases the adhesive force (e.g., about one order of magnitude at 0.1 and 0.2 M).

Fig. 9 compares the hydrodynamic torques (T_D) that the heteroaggregate in Fig. 1 and the large sphere of the heteroaggregate experience on the planar surface at different flow velocities with the adhesive torques that they experience at 0.2 M. The range of flow velocity (i.e., 7×10^{-6} to 2×10^{-3} m/s) considered is relevant to the processes in natural and engineered aquatic systems [66]. The hydrodynamic torque T_D experienced by a particle in the vicinity of the collector surface due to hydrodynamic shear is expressed as follows [45]:

$$T_D = 1.4 a_p F_D \tag{5}$$

where a_p is particle radius, F_D is the drag force experienced by an attached particle in a laminar flow field, written as Burdick et al. [11].

$$F_D = 10.2\pi\mu a_p V_p \tag{6}$$

where μ is fluid viscosity, V_p is the relative velocity between the fluid and the particle at the center of the particle. The adhesive torque (T_A) is represented by the adhesive force (F_A) acting on a level arm l_c:

$$T_A = F_A l_c \tag{7}$$

The level arm l_c is provided by the radius of particle–surface contact area (a_0), resulting from deformation of the particle. The equation to calculate a_0 is as follows [36].

$$a_0 = \left(\frac{F_A a_p}{4E}\right)^{1/3} \tag{8}$$

where E is elastic interaction constant. A value of 4.0×10^9 N m^{-2} was taken for the elastic interaction constant for the glass collectors and polystyrene particle suspensions [6,40,64]. Fig. 9 shows that the adhesive torque that the large sphere of the heteroaggregate experiences on the planar surface is even greater than the maximum hydrodynamic torque. This is why the colloid filtration theory considers particle attachment at primary minima as a very fast immobilization process (i.e., the perfect sink model) by assuming that the strong attraction that the particle experiences at primary minima dominates over other applied forces (e.g., the hydrodynamic drag) [54]. However, if the microparticle is covered by nanoparticles,

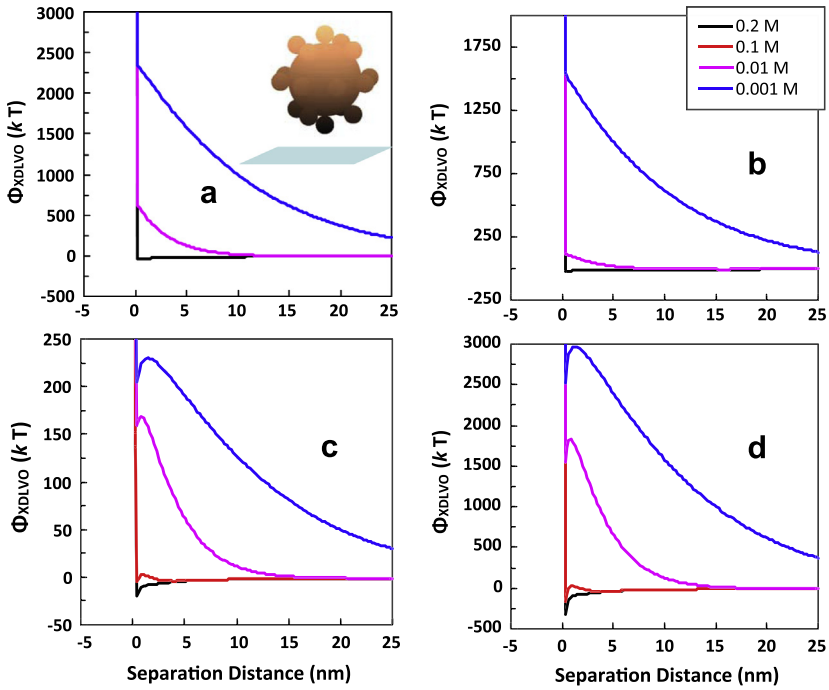

Fig. 6. DLVO interaction energies between the planar surface and the aggregate IV in Fig. 1 at different ionic strengths. The orientation of the aggregate is represented by the coordinates of the contacts between each small sphere and the large sphere in Table 1. The diameter of the large sphere is 1000 nm and the diameters of the small spheres are 5 nm, 10 nm, and 100 nm in (a–c), respectively. (d) shows the DLVO interaction energies between the planar surface and a sphere with a diameter of 1000 nm. Some of the curves at 0.1 M were not shown due to overlapping with the curves at other ionic strengths. Note the change in scale of the y axes among the various graphs.

the adhesive torque is greatly reduced and the attached aggregate at primary minima can be readily detached by the hydrodynamic drags commonly encountered in natural and engineered aquatic systems.

4. Discussion

If the coated nanoparticles are regarded as rough asperities on the microparticles, results of this study can be used to explain the detachment behavior of rough particles. Particularly, detachment of a rough particle from primary minimum will occur if the adhesion between the planar surface and the nanoscale rough asperity nearest to the planar surface is eliminated by the repulsion between the planar surface and the main body of the rough particle. Therefore, whereas it has been widely recognized that the presence of roughness on particle surface can decrease interaction energy barrier and accordingly increase attachment in primary minima [39,61,62,8,9,17,47,48,28,29,19,38], results in this study suggest that the nanoscale roughness on particle surfaces also favors particle detachment from primary minima upon reduction in solution ionic strength.

It is commonly believed that particle attachment in primary minima is irreversible to reduction in solution ionic strength because according to classic DLVO theory, the depth of the primary minimum increases with decreasing ionic strength and the potential interaction energy function increases more rapidly (representing a stronger attractive force) from zero separation distance at lower ionic strength [25,26]. In contrast, the DLVO theory shows that secondary minimum depth decreases with decreasing solution ionic strength. Therefore, the experimentally observed release of particles is commonly attributed to the detachment of those initially attached at secondary minima [50,67,57]. However, a number of studies [3,53,51,79,65,58,59], allowing particles to unambiguously attach in primary minima, found that the attached particles can be detached from primary minima upon reduction in solution ionic strength. Therefore, discrepancies exist between the observations and the prediction by the classic DLVO theory. The results in this study provide plausible explanation for the discrepancies.

Whereas the heteroaggregate was considered as a microparticle covered by nanoparticles (i.e., the heteroaggregate in Fig. 1), results of this study could be applicable for more complex heteroaggregates and rough particles. Particularly, detachment from primary minima will occur if the adhesion between the substrate and the primary sphere of the aggregate nearest the substrate or the rough asperity (not only spherical) is eliminated by the repulsion from the main body of the aggregate or the rough particle (not only micro-sized), For example, our study explains why viruses exhibit most conservative transport compared to microbial pathogens in the environments although the classic DLVO model predicts that smaller particles have lower interaction energy barriers and hence are more favored to be irreversibly attached at primary minima. This is because virus surfaces (i.e., capsid) are commonly rough (e.g., spikes on Coronavirus). The surface protrusions not only favor virus attachment, but also facilitate hydrodynamic and chemical detachment of viruses. Therefore, viruses can be continuously captured and released in the environment, causing traveling distances much farther than the predictions by irreversible models.

Similar to attachment, aggregation of particles at primary minima has been commonly regarded as a permanently irreversible contact between particles [33], and redispersion of aggregated particles is attributed to disassociation of particles from secondary minima [12,46,35,4,15,73]. The theoretical results in this study, however, suggest that the presence of nanoparticles or nanoscale roughness may cause repulsion between microparticles at all separation distances at low ionic strengths. As such, aggregation is inhibited. Indeed, Tohver et al. [63] found that whereas silica microspheres flocculate when suspended alone in aqueous solution, the addition of 6 nm zirconia nanoparticles could stabilize the microparticles. Viota et al. [69] showed that addition of 8 nm

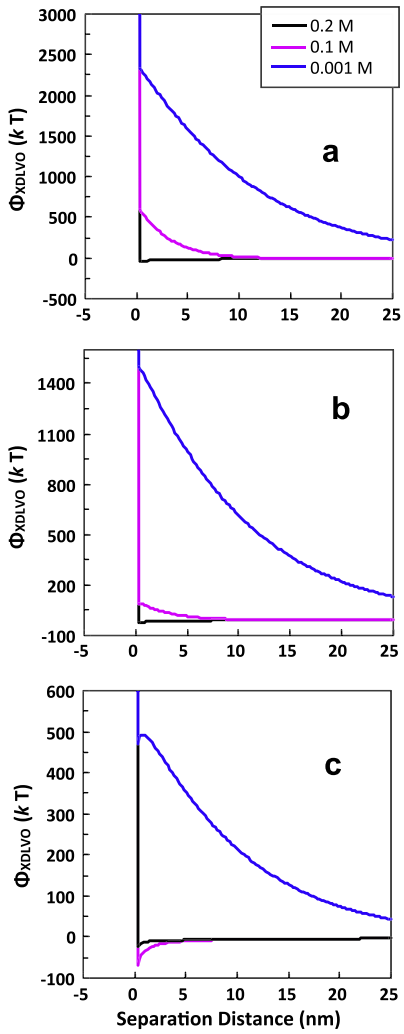

Fig. 7. DLVO interaction energies between the planar surface and the aggregate IV in Fig. 1 at different ionic strengths. The orientation of the aggregate is represented by the coordinates of the contacts between each small sphere and the large sphere in Table 1. The small particles of the aggregates are positively charged, with zeta potentials same as those of alumina in Fuerstenau and Pradip [23]. The diameter of the large sphere is 1000 nm and the diameters of the small spheres are 5 nm, 10 nm, and 20 nm in (a–c), respectively. Note the change in scale of the *y* axes among the various graphs.

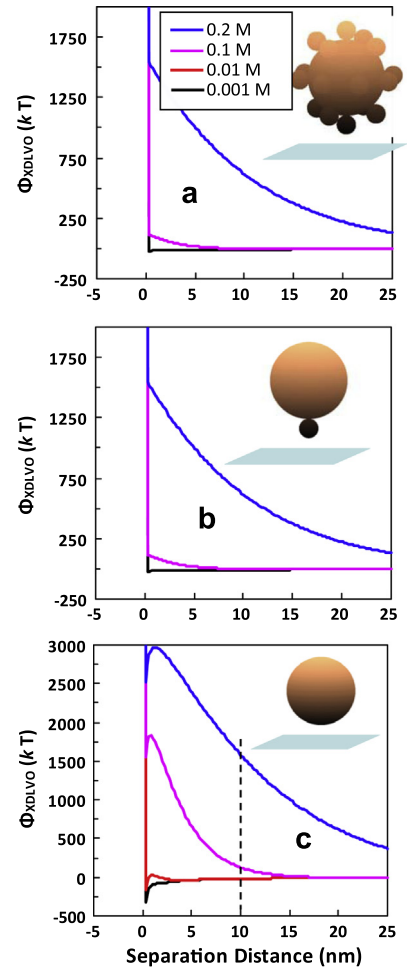

Fig. 8. DLVO energies for the interactions of the planar surface with (a) aggregate IV in Fig. 1, (b) the large sphere of the aggregate IV with one small sphere at the bottom, and (c) the large sphere only at different ionic strengths. The diameter of the large sphere in (a–c) is 1000 nm and the diameter of the small spheres in (a and b) is 10 nm. Some of the curves at 0.1 M were not shown due to overlapping with the curves at other ionic strengths. Note the change in scale of the y axes among the various graphs.

magnetite particles could improve the stability of 1450 nm magnetite particle suspensions.

Although this study used constant surface potential expression to calculate double layer interaction energies, results of study does not change if constant surface charge expression is used. This is because although the value of double layer interaction energy changes with using different expressions, the trend for the variation in interaction energy with ionic strength does not change for the homoaggregates or heteroaggregates. This study only adopted specific values for the Born collision diameter and Hamaker constant to calculate Born potential energy. Particle detachment from primary minimum will be enhanced with increasing Born collision parameter value and Hamaker constant value. In addition, our study considered that the interactions between aggregates and planar surface are nonspecific. Detachment could be reduced or even prevented if specific interactions (e.g., hydrophobic interaction) are present. We assumed that the particles are irreversibly aggregated. The aggregates may be redispersed during their detachment from surfaces if the particles are reversibly associated.

Table 2
Coordinates of the centers of the sphere centers for aggregate I with four orientations in Fig. 3. *r*, radius of the primary particles.

	x	*y*	*z*
Orientation in Fig. 3a	0	0	0
	$2r$	0	0
	r	$r\sqrt{26}/3$	$r/3$
	r	$r\frac{\sqrt{26}-2\sqrt{2}}{9}$	$r\sqrt{3-\left(\frac{\sqrt{26}-2\sqrt{2}}{9}\right)^2}$
Orientation in Fig. 3b	0	0	0
	$2r$	0	0
	r	$r\sqrt{10}/2$	$r\sqrt{2}/2$
	r	$r\frac{\sqrt{10}-4}{6}$	$r\sqrt{3-\left(\frac{\sqrt{4}-10}{6}\right)^2}$
Orientation in Fig. 3c	0	0	0
	r	$r\sqrt{26}/3$	$r/3$
	$-r$	$r\sqrt{26}/3$	$r/3$
	0	$r\frac{2\sqrt{26}-2\sqrt{2}}{9}$	$r\sqrt{4-\left(\frac{2\sqrt{26}-2\sqrt{2}}{9}\right)^2}$
Orientation in Fig. 3d	0	0	0
	r	$r\sqrt{10}/2$	$r\sqrt{2}/2$
	$-r$	$r\sqrt{10}/2$	$r\sqrt{2}/2$
	0	$r\frac{\sqrt{10}-2}{3}$	$r\sqrt{4-\left(\frac{\sqrt{10}-2}{3}\right)^2}$

Table 3
Calculated adhesive forces (F_A, N) that the aggregate IV and the large sphere of aggregate IV experience at different ionic strengths using the DLVO interaction energy curves in Fig. 6.

Ionic strength (M)	Aggregate IV with small spheres of 5 nm diameter	Aggregate IV with small spheres of 10 nm diameter	The large sphere of aggregate IV (N)
0.001	NA[a]	NA[a]	7.01×10^{-9}
0.01	NA[a]	NA[a]	4.38×10^{-9}
0.1	5.43×10^{-10} N	3.07×10^{-10} N	3.07×10^{-9}
0.2	5.92×10^{-10} N	3.24×10^{-10} N	5.19×10^{-9}

[a] Not applicable: no primary minimum existing in the DLVO interaction energy profiles.

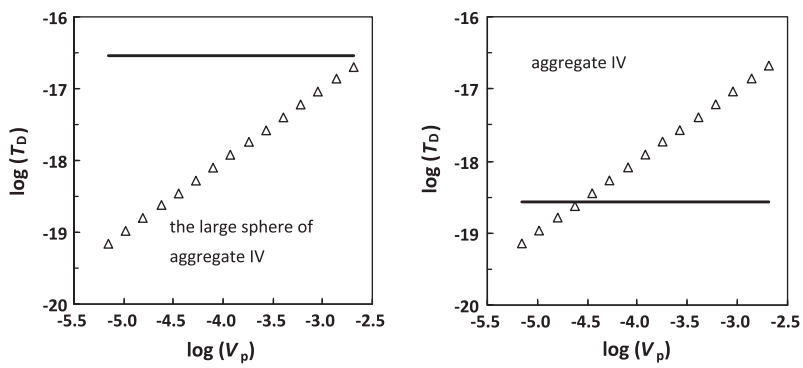

Fig. 9. Comparison of the adhesive torques T_A (solid line) that the aggregate IV and the large sphere of aggregate IV experience on the planar surface at 0.2 M with the hydrodynamic torques T_D (triangle) that they experience at different flow velocities. The diameters of the large sphere and small spheres for the aggregate IV are 1000 nm and 5 nm, respectively.

Investigating the co-present disaggregation and detachment is an ongoing topic but beyond the scope of this study.

5. Conclusions

In the subsurface environments, the released engineered nanoparticles (e.g., fullerene, carbon nanotube) or natural nanoparticles (e.g., clay soil) are likely to aggregate into clusters. The nanoparticles may also interact with larger particles such as bacteria and protozoa, resulting in heteroaggregates. The fate and transport of the formed aggregates have received limited attention to date. In particular, the detachment of the aggregates from collector surfaces during transients in solution chemistry has not been investigated. This study thus theoretically examined detachment of homoaggregates and heteroaggregates from planar surface using surface element integration. We showed that attached homoaggregates in primary minima are irreversible to reduction in solution ionic strength whether the primary particles of the homoaggregates are nano-sized or micro-sized. The attachment of nanoparticles on microparticles, however, can cause the interaction energy between the planar surface and the formed heteroaggregates to decrease monotonically with separation distance at low ionic strengths (e.g., $\leqslant$0.01 M), indicating that the heteroaggregates experience repulsive forces at all separation distances. Therefore, the attached heteroaggregates in primary minima at high ionic strengths (e.g., >0.1 M) can be detached upon reduction in ionic strength. Additionally, we showed that the adhesive forces and torques that the microparticles coated with nanoparticles experience are significantly smaller than those that the single microparticles experience and, thus, are readily detached from primary minima by hydrodynamic torque. Results of this study provide plausible explanation for the observed detachment/disaggregation of particles from primary minima upon reduction in solution ionic strength in the literature. Findings from this study also explain why viruses exhibit most conservative transport compared to microbial pathogens in the environments although the classic DLVO model predicts that smaller particles have lower interaction energy barriers and are favored to be irreversibly attached at primary minima.

Acknowledgments

We acknowledge the financial support provided by the National Natural Science Foundation of China (No. 41271009), Program for New Century Excellent Talents in University (NCET-13-0560), and National Key Technology R&D Program (No. 2012BAD05B02).

References

[1] S. Aramrak, M. Flury, J.B. Harsh, Langmuir 27 (2011) 9985–9993.
[2] R.C. Bales, S.R. Hinkle, T.W. Kroeger, K. Stocking, Environ. Sci. Technol. 25 (1991) 2088–2095.
[3] R.C. Bales, S. Li, Water Resour. Res. 29 (1993) 957–963.
[4] S.H. Behrens, D.I. Christl, R. Emmerzael, P. Schurtenberger, M. Borkovec, Langmuir 16 (2000) 2566–2575.
[5] J. Bergendahl, D. Grasso, AIChE J. 45 (1999) 475–484.
[6] J. Bergendahl, D. Grasso, Chem. Eng. Sci. 55 (2000) 1523–1532.
[7] J. Bergendahl, D. Grasso, Environ. Sci. Technol. 37 (2003) 2317–2322.
[8] S. Bhattacharjee, M. Elimelech, J. Colloid Interface Sci. 193 (1997) 273–285.
[9] S. Bhattacharjee, C.-H. Ko, M. Elimelech, Langmuir 14 (1998) 3365–3375.
[10] S.A. Bradford, S.R. Yates, M. Bettahar, J. Simunek, Water Resour. Res. 38 (2002) 1327–1339.
[11] G.M. Burdick, N.S. Berman, S.P. Beaudoin, Thin Solid Films 488 (2005) 116–123.
[12] D.Y.C. Chan, B. Halle, J. Colloid Interface Sci. 102 (1984) 400–409.
[13] N. Chatterjee, S. Lapin, M. Flury, Environ. Sci. Technol. 46 (2012) 4411–4418.
[14] K.L. Chen, M. Elimelech, Langmuir 22 (2006) 10994–11001.
[15] C.-J. Chin, S. Yiacoumi, C. Tsouris, S. Relle, S.B. Grant, Langmuir 16 (2000) 3641–3650.
[16] O.C. Compton, F.E. Osterloh, J. Am. Chem. Soc. 129 (2007) 7793–7798.
[17] K. Cooper, N. Ohler, A. Gupta, S. Beaudoin, J. Colloid Interface Sci. 222 (2000) 63–74.
[18] J. Czarnecki, Adv. Colloid Interface Sci. 24 (1985) 283–319.
[19] S. Eichenlaub, A. Gelb, S. Beaudoin, J. Colloid Interface Sci. 280 (2004) 289–298.
[20] M. Elimelech, C.R. O'Melia, Langmuir 6 (1990) 1153–1163.
[21] M. Elimelech, C.R. O'Melia, Environ. Sci. Technol. 24 (1990) 1528–1536.

[22] M. Elimelech, J. Gregory, X. Jia, R.A. Williams, Particle Deposition and Aggregation: Measurement, Modeling, and Simulation, Butterworth-Heinemann, Oxford, 1995.
[23] D.W. Fuerstenau, Pradip, Adv. Colloid Interface Sci. 114–115 (2005) 9–26.
[24] J. Gregory, Adv. Colloid Interface Sci. 147–148 (2009) 109–123.
[25] M.W. Hahn, C.R. O'Melia, Environ. Sci. Technol. 38 (2004) 210–220.
[26] M.W. Hahn, D. Abadzic, C.R. O'Melia, Environ. Sci. Technol. 38 (2004) 5915–5924.
[27] H.C. Hamaker, Physica 4 (1937) 1058–1072.
[28] C. Henry, J.-P. Minier, G. Lefevre, O. Hurisse, Langmuir 27 (2011) 4603–4612.
[29] E.M.V. Hoek, S. Bhattacharjee, M. Elimelech, Langmuir 19 (2003) 4836–4847.
[30] R.I. Hogg, T.W. Healy, D.W. Fuerstenau, Trans. Faraday Soc. 62 (1966) 1638–1651.
[31] E.M. Hotze, T. Phenrat, G.V. Lowry, J. Environ. Qual. 39 (2010) 1909–1924.
[32] X. Huang, S. Bhattacharjee, E.M.V. Hoek, Langmuir 26 (2010) 2528–2537.
[33] A.M. Islam, B.Z. Chowdhry, M.J. Snowden, Adv. Colloid Interface Sci. 62 (1995) 109–136.
[34] J.N. Israelachvili, Intermolecular and Surface Forces, second ed., Academic, London, 1992.
[35] G.C. Jeffrey, R.H. Ottewill, Colloid Polym. Sci. 266 (1988) 173–179.
[36] K.L. Johnson, Contact Mechanics, Cambridge University Press, Cambridge, 1985.
[37] C.P. Johnson, X. Li, B.E. Logan, Environ. Sci. Technol. 30 (1996) 1911–1918.
[38] J. Katainen, M. Paajanen, E. Ahtola, V. Pore, J. Lahtinen, J. Colloid Interface Sci. 304 (2006) 524–529.
[39] A.M. Lenhof, Colloids Surf., A 87 (1994) 49–59.
[40] X. Li, P. Zhang, C.L. Lin, W.P. Johnson, Environ. Sci. Technol. 39 (2005) 4012–4020.
[41] S. Lin, M.R. Wiesner, Environ. Sci. Technol. 46 (2012) 13270–13277.
[42] G.V. Lowry, K.B. Gregory, S.C. Apte, J.R. Lead, Environ. Sci. Technol. 46 (2012) 6893–6899.
[43] V.N. Manoharan, M.T. Elsesser, D.J. Pine, Science 301 (2003) 483–487.
[44] B.W. Ninham, Adv. Colloid Interface Sci. 83 (1999) 1–17.
[45] M.E. O'Neill, Chem. Eng. Sci. 23 (1968) 1293–1298.
[46] N.H.G. Penners, L.K. Koopal, Colloids Surf. 28 (1987) 67–83.
[47] Y.I. Rabinovich, J.J. Adler, A. Ata, R.K. Singh, B.M. Moudgil, J. Colloid Interface Sci. 232 (2000) 10–16.
[48] Y.I. Rabinovich, J.J. Adler, A. Ata, R.K. Singh, B.M. Moudgil, J. Colloid Interface Sci. 232 (2000) 17–24.
[49] R. Rajagopalan, C. Tien, AIChE J. 2 (1976) 523–533.
[50] J.A. Redman, S.L. Walker, M. Elimelech, Environ. Sci. Technol. 38 (2004) 1777–1785.
[51] S.B. Roy, D.A. Dzombak, Colloids Surf., A 119 (1996) 133–139.
[52] E. Ruckenstein, D.C. Prieve, AIChE J. 22 (1976) 276–283.
[53] J.N. Ryan, P.M. Gschwend, Environ. Sci. Technol. 28 (1994) 1717–1726.
[54] J.N. Ryan, M. Elimelech, Colloids Surf., A 107 (1996) 1–56.
[55] N.B. Schade, M.C. Holmes-Cerfon, E.R. Chen, D. Aronzon, J.W. Collins, J.A. Fan, F. Capasso, V.N. Manoharan, Phys. Rev. Lett. 110 (2013) 148303.
[56] J.F. Schijven, S.M. Hassanizadeh, Crit. Rev. Environ. Sci. Technol. 30 (2000) 49–127.
[57] C. Shen, B. Li, Y. Huang, Y. Jin, Environ. Sci. Technol. 41 (2007) 6976–6982.
[58] C. Shen, V. Lazouskaya, Y. Jin, B. Li, Z. Ma, W. Zheng, Y. Huang, J. Contam. Hydrol. 134–135 (2012) 1–11.
[59] C. Shen, F. Wang, B. Li, Y. Jin, L.-P. Wang, Y. Huang, Langmuir 28 (2012) 14681–14692.
[60] C. Shen, V. Lazouskaya, H. Zhang, B. Li, Y. Jin, Y. Huang, Colloids Surf., A 433 (2013) 14–29.
[61] L. Suresh, J.Y. Walz, J. Colloid Interface Sci. 183 (1996) 199–213.
[62] L. Suresh, J.Y. Walz, J. Colloid Interface Sci. 196 (1997) 177–190.
[63] V. Tohver, J.E. Smay, A. Braem, P.V. Braun, J.A. Lewis, PNAS 98 (2001) 8950–8954.
[64] S. Torkzaban, S.A. Bradford, S.L. Walker, Langmuir 23 (2007) 9652–9660.
[65] T. Tosco, A. Tiraferri, R. Sethi, Environ. Sci. Technol. 43 (2009) 4425–4431.
[66] N. Tufenkji, M. Elimelech, Environ. Sci. Technol. 38 (2004) 529–536.
[67] N. Tufenkji, M. Elimelech, Langmuir 21 (2005) 841–852.
[68] E.J.W. Verwey, J.Th.G. Overbeek, Theory of the Stability of Lyophobic Colloids, Elsevier, Amsterdam, 1948.
[69] J.L. Viota, F. Gonzalez-Caballero, J.D.C. Duran, A.V. Delgado, J. Colloid Interface Sci. 309 (2007) 135–139.
[70] Y. Wang, Y. Li, K.D. Pennell, Environ. Toxicol. Chem. 27 (2008) 1860–1867.
[71] Y. Wang, Y. Wang, D.R. Breed, V.N. Manoharan, L. Feng, A.D. Hollingsworth, M. Weck, D.J. Pine, Nature 491 (2012) 51–55.
[72] M. Weiss, Y. Luthi, J. Ricka, T. Jorg, H. Bebie, J. Colloid Interface Sci. 206 (1998) 322–331.
[73] K.L. Wu, S.K. Lai, Langmuir 21 (2005) 3238–3246.
[74] L. Wu, B. Gao, Y. Tian, R. Munoz-Carpena, K.J. Zigler, Langmuir 29 (2013) 3976–3988.
[75] K.M. Yao, M.T. Habibian, C.R. O'Melia, Environ. Sci. Technol. 5 (1971) 1105–1112.
[76] G.-R. Yi, V.N. Manoharan, E. Michel, M.T. Elsesser, S.-M. Yang, D.J. Pine, Adv. Mater. 16 (2004) 1204–1206.
[77] G.-R. Yi, D.J. Pine, S. Sacanna, J. Phys.: Condens. Matter 25 (2013) 193101.
[78] D. Zerrouki, B. Rotenberg, S. Abramson, J. Baudry, C. Goubault, F. Leal-Calderon, D.J. Pine, J. Bibette, Langmuir 22 (2006) 57–62.
[79] J. Zhang, S. Srivastava, R. Duffadar, J.M. Davis, V.M. Rotello, M.M. Santore, Langmuir 24 (2008) 6404–6408.